CREEP BEHAVIOUR OF CRACKED STEEL FIBRE REINFORCED SELF-COMPACTING CONCRETE: FROM MICRO-MECHANICS TO COMPOSITE BEHAVIOUR

Amin Abrishambaf[*1], *Joaquim A. O. Barros*[1], *and Vitor M.C.F. Cunha*[1]

[1] *ISISE, Dep. Civil Eng., School Eng., University of Minho, Campus de Azurém 4800-058 Guimarães, Portugal.*

ABSTRACT

This work presents the results of an extensive experimental program that aims to study the long-term behaviour of cracked steel fibre reinforced self-compacting concrete (SFRSCC). At the micro-level, a series of single fibre pull-out creep tests were performed, and the fibre slip was monitored as a function of time. The influence of fibre orientation angle (0, 30 and 60 degrees), as well as pre-imposed fibre slip levels 0.3 and 0.5 mm on the creep behaviour was investigated. At the composite level, prismatic specimens were extracted from a SFRSCC panel, having in consideration the concrete flow direction. The specimens were pre-cracked up to 0.3 and 0.5 mm and subjected to a sustained flexural loading. In this stage, the influence of the pre-crack level and fibre orientation on the long-term crack opening was appraised. Furthermore, instantaneous fibre pull-out tests and bending tests were performed on undamaged specimens to quantify the effects of the creep phenomenon. It was found that a higher damage level in the specimens accelerated the creep rate. Moreover, the creep performance of the SFRSCC was influenced by the fibre orientation. Finally, the assembled creep curves did not differ considerably from the instantaneous behaviours for the adopted pre-damaged levels.

Keywords: Time-dependent behaviour; Long-term load; Creep; Rheology; Steel fibre reinforced self-compacting concrete.

* Amin Abrishambaf, PhD, ISISE
University of Minho
Campus de Azurém
Guimaraes, 4800-058
Portugal

Email: amabrishambaf@gmail.com
Tel: +351 253 510 210

1. INTRODUCTION

Discrete fibres are increasingly being used in the construction industry to overcome the brittle nature of plain concrete under tension, and either to avoid or reduce the use of conventional steel reinforcement. In fibre reinforced concrete (FRC) macro-cracks that arise within the cementitious matrix are bridged by fibres randomly distributed in the concrete. It is widely acknowledge that the mechanical behaviour of steel fibre reinforced self-compacting concrete (SFRSCC) depends not only on the bond behaviour of the fibre/matrix interface, but also on both fibre's distribution and orientation parameters [1-4]. Consequently, it is of utmost importance to understand the influence of fibre's distribution/orientation on the mechanical performance of FRC.

The long-term deformation of the composite could ultimately lead to the failure mechanism of the structural element at a load lower than static ultimate load [5]. The influence of creep will be adverse, if the long-term deformation significantly damages the fibre/matrix interface bond, thus leading to an undesirable excessive decrease of the post-cracking residual strengths [6]. On the other hand, in some structural systems, the creep deformation of the structural element can be beneficial, since it allows stresses to redistribute, which can limit the crack propagation. Creep in a cracked steel fibre reinforced concrete (SFRC) element under flexural loading is the result of the following phenomena: basic creep (concrete creep in compression); fibre creep at it's material level in tension; loss of fibre-matrix adherence and subsequent fibre free-sliding. In the case of using steel fibres as reinforcement, creep in the fibre can be neglected due to the relatively low shear level installed in most of the fibres within the matrix. Therefore, the long-term crack widening of SFRC can be mainly ascribed to the long-term sliding of fibre through its channel in matrix, which depends on several factors such as: quality of matrix, bond strength, fibre embedment length, fibre geometry, fibre anchorage mechanism, fibre orientation, etc. To sum it up, in order to predict the creep behaviour of a cracked SFRSCC element, it is essential to understand the long-term behaviour of the fibre/matrix interface bond at the micro-level.

This works describes the results of an extensive experimental program that aims to study the long-term behaviour of cracked SFRSCC from the micro-level to the composite behaviour. At the micro-level, a series of the single fibre pull-out creep tests were performed, and the fibre slip was monitored as a function of time. The influence of fibre orientation angle (0, 30 and 60 degrees), as well as pre-imposed fibre slip levels 0.3 and 0.5 mm on the creep behaviour was investigated. At the composite level, prismatic specimens were extracted from a SFRSCC panel, taking into account the concrete flow direction. The specimens were pre-cracked up to 0.3 and 0.5 mm and subjected to a sustained flexural loading. In this stage, the influence of pre-crack level and fibre orientation on the long-term crack opening was appraised. Furthermore, instantaneous fibre pull-out tests and bending tests were performed on undamaged specimens to quantify the effects of the creep phenomenon.

2. MICRO-MECHANICAL BEHAVIOUR

In this section, it is summarized the experimental long-term micro-mechanical behaviour of steel fibres embedded in a self-compacting concrete matrix. Further details can be found elsewhere [7].

2.1. Concrete mixture and specimens

Table 1 includes the composition of the developed self-compacting concrete. The concrete properties in the fresh state were determined by the Abrams cone slump test in the inverted position according to the recommendation of EFNARC [8], having been obtained an average spread of 590 mm. Hooked-end steel fibres with a length, l_f, of 33 mm; diameter, d_f, of 0.55 mm; aspect ratio, l_f / d_f , of 60 and yield stress of 1100 MPa, were used.

The compressive strength of the hardened concrete was assessed by testing six cylinders with a diameter of 150 mm and a height of 300 mm at the age of 28 days. The specimens were cast and stored in a climatic chamber room under 20ºC and 60% relative humidity. The average compressive strength was 72.3 MPa with a coefficient of variation (CoV) of 8.23 %, while the average Young's modulus was 42.1GPa with CoV of 0.26 %.

Table 1. Mix composition of self-compacting concrete per m^3.

Cement [kg]	Water [kg]	W/C [–]	SP [kg]	Limestone filler [kg]	Fine sand [kg]	Coarse sand [kg]	Coarse aggregate [kg]
413	124	0.30	7.83	353	237	710	590

The pull-out tests were performed on single-sided cylindrical specimens. A single steel fibre was embedded into a cylindrical concrete specimen with 80 mm in height and diameter. For this purpose, a mould allowing the production of 81 specimens at the same time ensuring a certain embedment length and orientation was used. Figure 1 shows the specimen's manufacturing procedure. In this study, 0, 30 and 60 degree fibre inclination angles were considered. Cunha *et al.* [9] determined that the influence of the fibre embedment length was not so significant as the orientation angle effect. Therefore, considering that the theoretical value of a fibre's embedded length bridging an active crack is $l_f/4$ = 8.25 mm [10], this value was selected as the fibre's embedment length in the production of all the specimens. For each orientation angle, six instantaneous and six long-term pull-out specimens were prepared (three for each pre-imposed fibre slip level, s_{pr}).

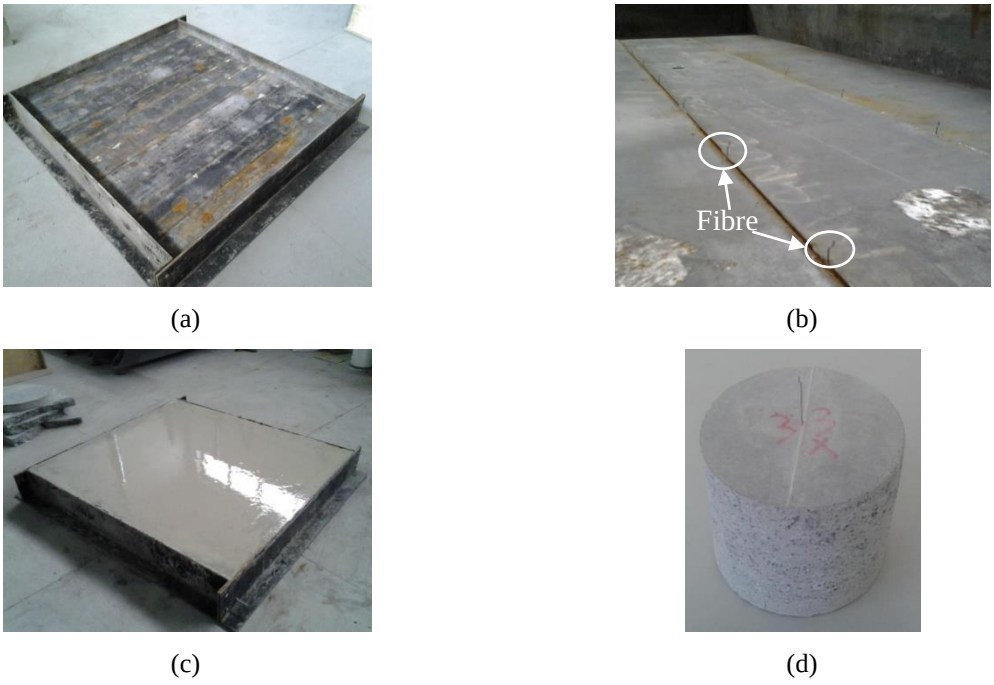

Figure 1. Production of the specimens for fibre pull-out test: (a) casting mould, (b) fibre positioning in the mould, (c) casting panel with SCC, and (d) extracted pull-out specimen.

2.2. Test set-up

2.2.1. Instantaneous fibre pull-out test

The instantaneous fibre pull-out load – slip relationship, *F* - *s*, was obtained using a universal testing rig with a load carrying capacity of 50 kN. However, a load cell with higher accuracy was used, namely, a HBM® type S9 load cell with a capacity of 5 kN to record pull-out load more accurately, see Figure 2(a). The specimens were tested at the age of 28 days.

For measuring the fibre's slip, three Linear Variable Differential Transformers (LVDTs) with linear stroke +/- 5 mm were installed on the back side of the grip using aluminium cubic supports to exclude measuring deformation of the test rig, Figure 2(b). Moreover, a VMS-004D-400x USB Microscope

camera with a 2 Mega Pixels resolution was also used to assess the fibre slip at the grip. The test was controlled by an LVDT installed on the actuator, and adopting a displacement rate of $1\ \mu m/s$ up to the slip of 2 mm, and $4\ \mu m/s$ until the end of the test. This test control procedure guaranteed a stable response during the test, particularly during the debonding process of the fibre.

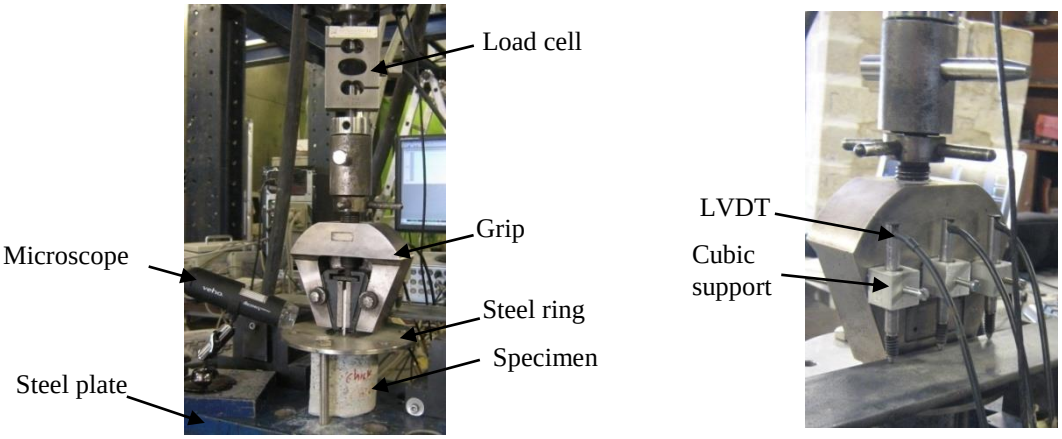

Figure 2. Configuration of the single fibre pull-out test: (a) test components and (b) connection of LVDT.

2.2.2. Long-term fibre pull-out test

The long-term fibre pull-out tests were carried out in three stages: firstly, the fibres were exposed to a pre-slip level of either 0.3 or 0.5 mm; secondly, the creep tests were performed on the pre-imposed fibre slip specimens until the stabilization of the long-term slip; and finally, monotonic pull-out tests were performed until the fibre was fully pulled-out.

Pre-slipping stage

The monotonic pull-out test set-up was adapted to pre-slip the fibres. The fibre was loaded until the average slip in the LVDTs reached a certain pre-slip level, s_{pr}, (the load at this slip level is designated as F_{pr}) and then the specimen was unloaded. In this study, two nominal slip levels were investigated: 0.3 mm that can be correlated to the crack opening width in serviceability limit states, and 0.5 mm that was close to the peak pull-out load.

Pull-out creep stage

For evaluating the long-term performance of fibre/matrix interface, an innovative test setup that was conceived and designed by Costa and Barros (2015) [11] adjusted to allow testing five specimens simultaneously (Figure 3). During the creep test, the fibre slip was obtained with an LVDT installed on each grip. To evaluate the level of fibre slippage at the grip, a USB Microscope was also used. In this test, at the time of loading and unloading procedures the slip was measured within a relatively short time period (one reading per 2 sec) since the slip variation was significant at this stage. To reduce the size of the recorded data, the read-outs were saved with a lower frequency, one read-out per 500 and 1000 seconds for the first month and until the completion of the test, respectively.

After the initiation of the creep test, the value of the applied load, F_a, was maintained constant until the long-term slip was stabilized. When the variation of the long-term slip was smaller than one micrometer for three consecutive days, it was assumed that the slip was stabilized, and the test was finalized. In the present research, it was opted to apply a load level (F_a / F_{pr}) equal to 100 or 80% of that observed at s_{pr}=0.3 or 0.5 mm in the pre-slip tests, respectively. After the conclusion of the creep tests, the specimens were unloaded, but the data acquisition system was kept active for at least a period of one week, enabling to record the recoverable slip component due to the creep recovery process.

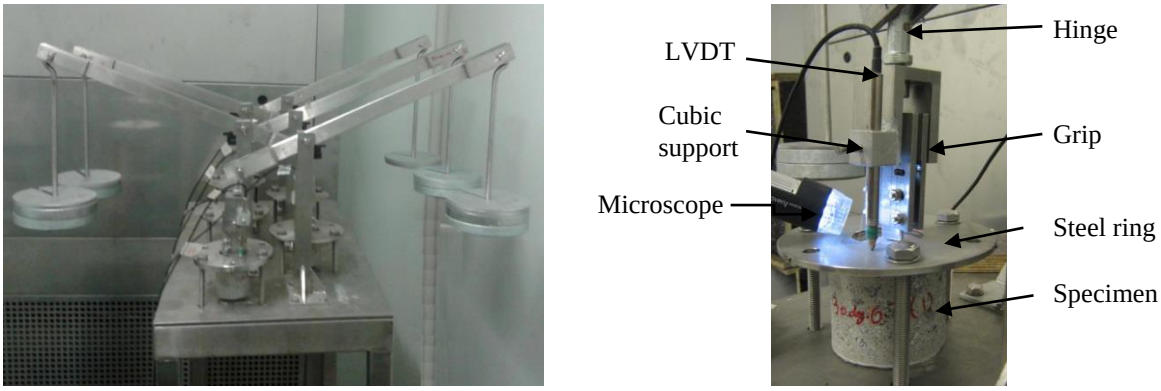

(a) (b)

Figure 3. Fibre pull-out creep test set-up: (a) general view and (b) specimen installation details.

Post-creep stage

The specimens were then subjected to a monotonic fibre pull-out test, one week after the creep tests have finished. The monotonic test set-up was same as to the one used for pre-slipping the fibres, which was already detailed.

2.3. Results and discussion

2.3.1. Instantaneous fibre pull-out tests

Figure 4 shows the average pull-out load – slip relationships and correspondent envelopes for the adopted fibre inclinations.

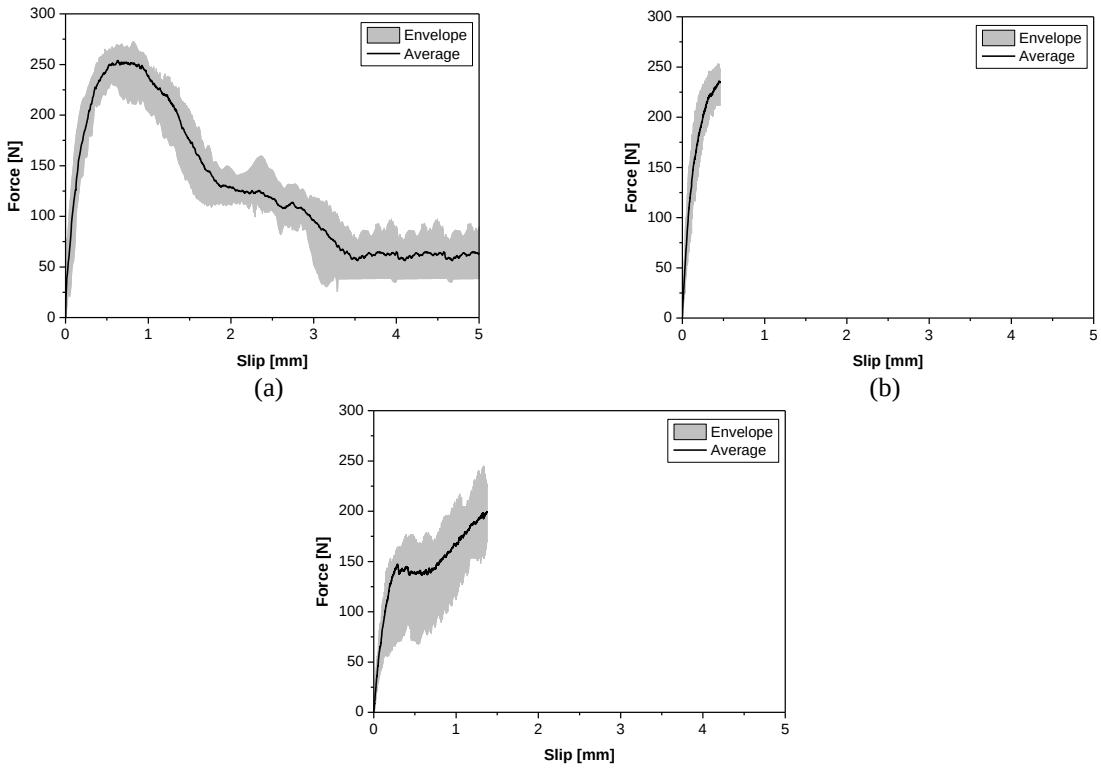

(a) (b)

(c)

Figure 4. Average instantaneous pull-out load versus slip relationships for fibre inclination angles of: (a) 0°, (b) 30° and (c) 60°.

For the fibres with an inclination angle of 0°, the pre-peak branch consists of a linear and nonlinear part. The linear part corresponds to the elastic behaviour of the bond, whereas the nonlinear part could be ascribed to a mix of two mechanisms: degradation of the adhesion between the fibre and surrounding matrix, and the beginning of the end hook's mobilization process. After the peak load is attained, both curvatures of the hooked end are progressively deformed and thus, the pull-out load starts to decrease up to a slip of 3.5 mm. Finally, after the hook has been fully straightened, the pull-out process has occurred under frictional resistance. Figure 4(b) depicts the pull-out load versus slip curve for fibres with an inclination angle of 30°. The pre-peak branch is similar to the fibres with 0° angle, but a slightly lower value of peak load was attained, and finally the fibre was ruptured. Figure 4(c) shows the pull-out load – slip relationship for the 60° specimens. In the first phase, the load has increased until the first evidence of matrix spalling. Afterwards, a matrix wedge was formed and gradually detached. After the completion of wedge spalling off, a new equilibrium was attained and the pull-out fibre process has continued with a lower stiffness until the fibre rupture.

2.3.2. Long-term fibre pull-out tests

Figure 5 shows the average and envelope of the long-term slip, s_{lt}, versus time for each fibre orientation angle and pre-slip level, up to a period of two months. As it was mentioned earlier, for s_{pr}=0.3 or 0.5 mm, the applied load level (F_a / F_{pr}) was 100 or 80% of that observed at in the pre-slip tests, respectively. For s_{pr} = 0.5 mm series, the creep test could not be performed on the specimens with a fibre inclination angle of 30°, because the fibres have ruptured during the execution of the monotonic pull-out tests at an average slip of 0.47 mm. All series have shown a two-stage creep response, namely, primary and secondary stages, in which the long-term slip has increased faster with time and then followed by a steady state part where the increment in slip was not so predominant. However, in s_{pr} = 0.5 mm series, the slip was stabilized in a higher time period. It should be worth noted that the former specimens subjected to a higher level of damage in the bond, therefore slip was stabilized in a higher time period. Under the sustained load, none of the specimens entered in the tertiary stage of the creep behaviour, i.e. unstable creep response, where long-term slip increases in time sharply until fully extraction of the fibre.

Comparing the responses depicted in Figure 5, it is visible that the fibre orientation has an important effect on the long-term slip, since a clear increase of s_{lt} with the decrease of fibre inclination was observed. This tendency seems to increase with the s_{pr} applied. In the s_{pr}= 0.3 mm series and fibre inclination angle of 0°, at 60 days' time, the long-term slip was 19% and 69% higher than in the case of fibre orientation angles of 30 and 60°, respectively, see Figure 5(a), (c), (e). Regarding the series s_{pr} = 0.5 mm, the fibre orientation effect is even more pronounced since at 60 days' time, the long-term slip of fibre at 0° was 135% larger than at 60°, see Figure 5(b), (f). The different failure modes observed in the specimens with fibres differently oriented can contribute for this behaviour. As it was observed from the monotonic pull-out test results, for specimens with inclination angle of 0°, the fibre was fully pulled-out, whereas for 30° and 60° orientation angels, the pull-out procedure was mainly governed by matrix spalling and finally fibre rupturing. From another point of view, for 0° series, s_{pr} = 0.5 mm was very close to the slip correspondent to the peak load, $s_p^{\max}$. On the other hand, by comparing the ratio of the applied load in creep test to the maximum load recorded during pull-out test, $F_a / F_p^{\max}$, in average terms, this coefficient was 81% and 39% for 0° and 60° orientation angles, respectively. Therefore, loading specimens in a level close to the maximum load carrying capacity of the specimen hastens the development of higher long-term slip under a sustained load.

Considering specimens with 0° fibre orientation angle (Figure 5(a) and (b)), the long-term slip increased significantly with s_{pr}. In s_{pr} = 0.5 mm specimens, the bond between the fibre/matrix had a higher level of damage, consequently it was observed a higher long-term slip due to the creep behaviour. An increase of 50% on the long-term slip was observed for the fibres pre-slipped up to 0.5 mm when compared to the s_{pr} = 0.3 mm series. On the other hand, the series with a 60° angle have shown a distinct behaviour, see Figure 5(e) and (f). By increasing the pre-slip from 0.3 mm to 0.5 mm, the long-term slip had a slight increase. From Figure 4(c) it is observed that both studied pre-slip levels were positioned in the plateau part of the monotonic pull-out response of the 60º series, in which the slip increased at an almost constant load. Therefore, the achieved pre-slipping load, F_{pr}, for

both investigated pre-slip levels was relatively similar. In the long-term pull-out tests for 60º series, considering the selected loading levels for each series, the specimens of the 0.5 mm series were subjected to a lower applied load, F_a. Hence, it is rational to expect that the creep response for this series exhibited a close response to the 0.3 mm series, even though s_{pr} =0.5 mm series endured a higher level of damage at the fibre/matrix interface.

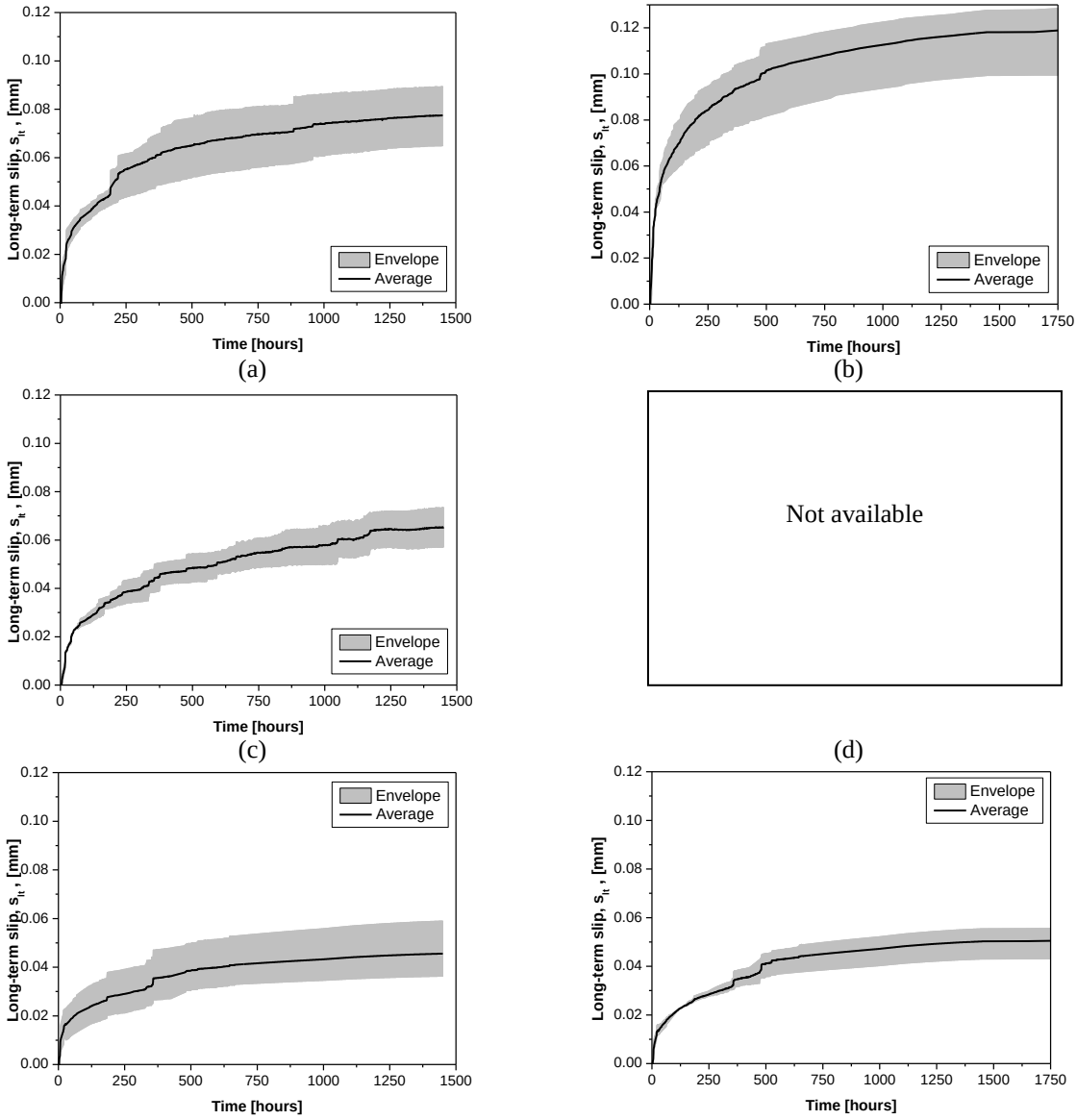

Figure 5. Long-term slip versus time during fibre pull-out creep test: (a) and (b) 0 degree, (c) and (d) 30 degree, (e) and (f) 60 degree; (a), (c), (e) s_{pr} = 0.3 mm and (b), (d), (f) s_{pr} = 0.5 mm.

2.3.3. Comparison between instantaneous and long-term results

Figure 6 includes both the instantaneous and long-term pull-out assembled curves for each fibre orientation and s_{pr}. These responses were obtained by averaging all the correspondent curves. The long-term assembled relationships consist of overlaying the force – slip curves from the tests corresponding to: the specimen's pre-slipping, creep, and post-creep tests. The development of the long-term slip has a minor influence on the post-creep residual forces. It is evident that the assembled curves resemble quite well the average responses of the instantaneous tests. Nevertheless, in some cases, due to the scatter of the test results, the assembled responses did not follow so closely the

average instantaneous curves, nonetheless they are yet comprised within the experimental envelope of the monotonic pull-out tests.

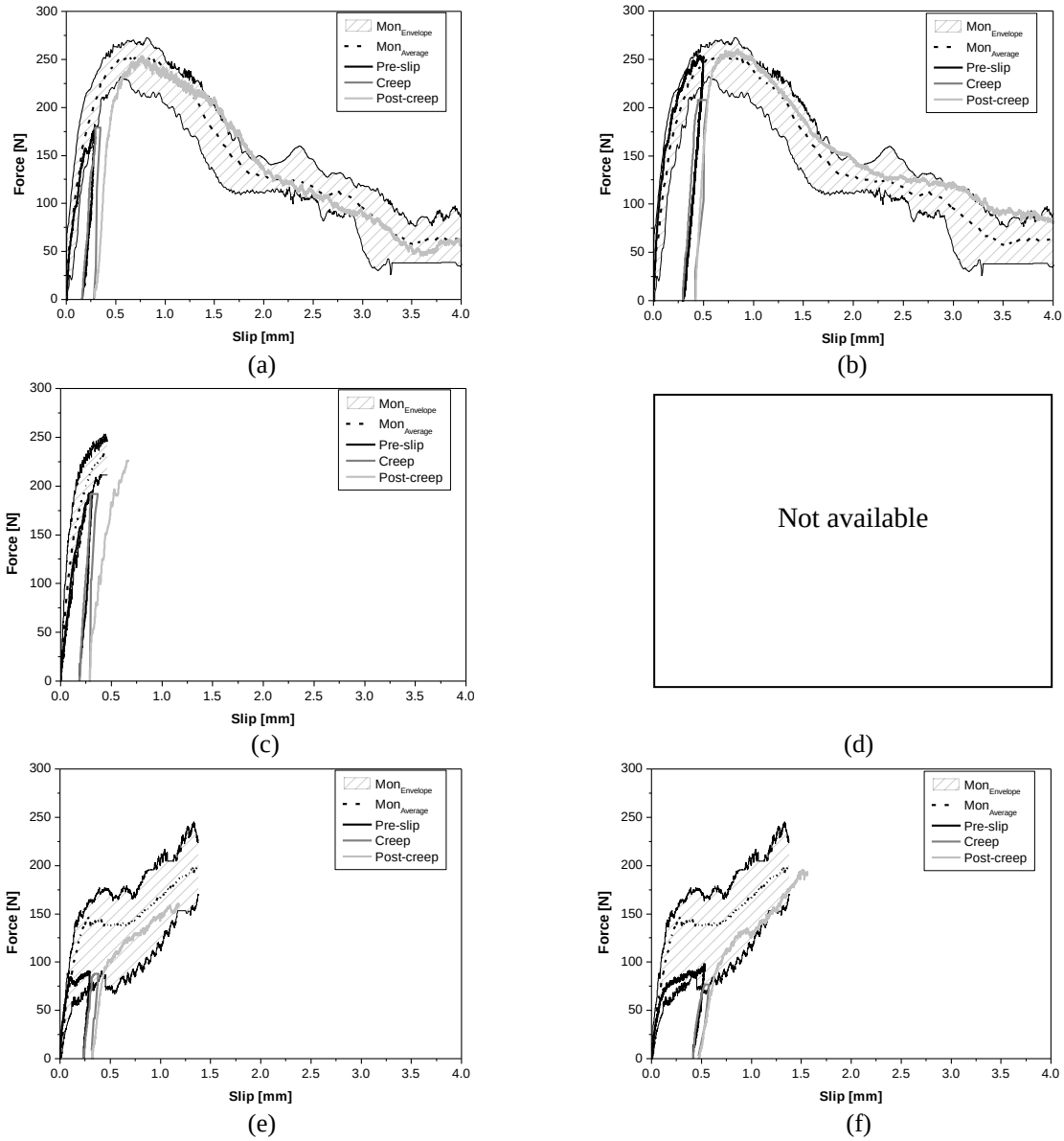

Figure 6. Comparison of instantaneous and long-term assembled curves: (a) and (b) 0 degree, (c) and (d) 30 degree, (e) and (f) 60 degree; (a), (c), (e)s_{pr}= 0.3 mm and (b), (d), (f) s_{pr} = 0.5 mm.

3. TENSILE BEHAVIOUR UNDER FLEXURE

In this section, a summary of the experimental long-term flexural behaviour of cracked SFRSCC specimens is presented and discussed. More details regarding these aspects can be found in [7].

3.1. Concrete mixture and specimens

A SFRSCC panel with the dimensions of 1500× 1500 mm^2 in plan and 60 mm of thickness was cast from its centre using the concrete composition presented in Table 1. A fibre content of 60 kg/m^3 was used. The steel fibres had the same characteristics of the ones used to assess the micro-mechanical behaviour. A total of one hundred and twelve prismatic specimens with the dimensions of 240×60×60

mm^3 were extracted from distinct locations of the panel, see Figure 7(a). In this scheme, the light grey solid hatched specimens were used for assessing the long-term behaviour, whereas the rest of the specimens were tested under instantaneous monotonic load conditions at the same age of the specimens cracked for the creep test. After the extraction of the prismatic specimens, a notch was executed at mid span. The notch depth and thickness were 10 and 2 mm, respectively.

The orientation of the notched plane was defined according to the following strategy: by considering β as the angle between the direction of the concrete flow and the notched plane direction, four series of prismatic specimens with different notched plane orientations towards the concrete flow directions were defined. Figure 7(b) depicts a scheme of the adopted classification methodology based on the angle β. The four intervals established for the angle β were [0-15°[, [15-45°[, [45-75°[and [75-90°]. Hereinafter, each series was designated by an alphanumeric string according to: in the case of the specimens for the long-term tests, the first character represents the distance from the casing point (L-Low: [0-375mm[; A-Average: [375-565 mm[and H-High: [565-750 mm]); the second numeral refers to the two studied pre-crack widths (w_{cr}), 0.3 and 0.5 mm; the third numeral defines the average β angle, in degrees, for four intervals of the relative orientation between the notched plane and the SFRSCC flow lines (7.5: [0-15°[, 30: [15-45°[, 60: [45-75°[and 82.5: [75-90°]), and the last numeral represents the number of the specimen. A similar strategy for designating the instantaneous monotonic test specimens was followed, however the second character that indicates the pre-crack width was ignored, since these tests were performed on uncracked specimens.

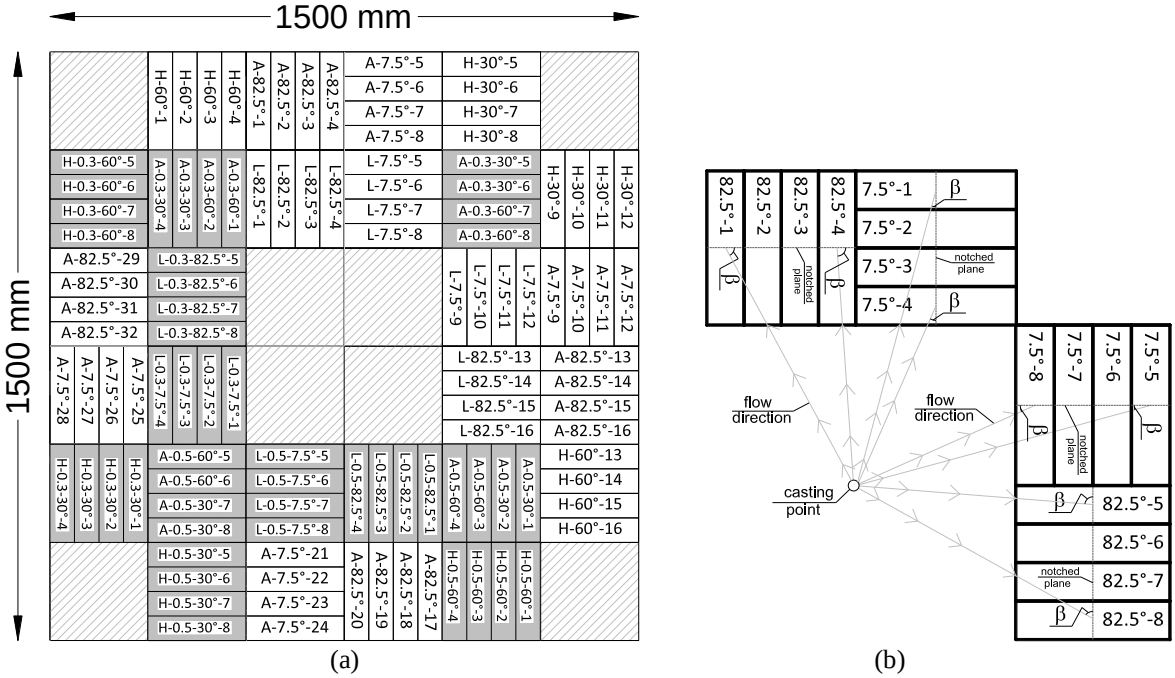

(a) (b)

Figure 7. (a) Specimen's extracting plane, (b) definition of β angle.

3.2. Test set-up

3.2.1. Instantaneous four-point bending test

The instantaneous Force - crack tip opening displacement, *F* – CTOD, relationship was determined from a total of sixty four monotonic four-point bending tests, performed on the specimens at the age of 28 days, following the recommendations of the Italian standard [12]. Figure 8 depicts the test set-up and geometry of the specimen. To determine the deflection during the test, a LVDT was mounted on an aluminium bar supported at mid height of the sections coinciding with the supports of the specimen in order to exclusively record the deflection of the specimen, see Figure 8(a). To assess an eventual asymmetric crack opening, due to fibre segregation along the panel's thickness, CTOD was determined from the readouts of three LVDTs on the beam's bottom surface, see Figure 8(b) and (c).

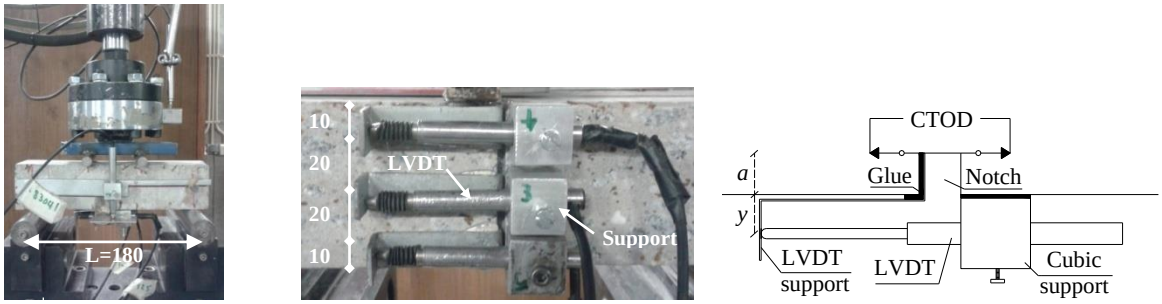

(a) (b) (c)

Figure 8. Test set-up of the monotonic four-point bending test (dimensions are in mm): (a) geometry of the specimen (b) LVDTs to determine CMOD, (c) LVDT connection details.

3.2.2. Long-term four-point bending test

In order to obtain the long-term Force - crack width relationship, $F - w$, experimental tests were carried out in three stages: firstly, the beams were pre-cracked up to a crack width of either 0.3 or 0.5 mm; secondly, the creep tests were carried out on the pre-cracked beams until the stabilization of the creep crack width has been achieved; finally, post-creep bending tests were performed until failure of the specimen.

Pre-cracking stage

In a first stage, the monotonic test set-up previously described was used to attain the desired crack opening width (w_{cr}). In this research, two initial crack opening widths were studied, namely, 0.3 mm, recommended for the serviceability limit state, and 0.5 mm that coincides to the crack opening width corresponding to the one used to compute the residual flexural strength, $f_{R,1}$ [13].

Creep stage

After finalizing the pre-cracking procedure, the specimens were carefully moved to the climate chamber room. The creep testing rig allowed loading simultaneously three specimens. Figure 9(a) shows the adopted creep test set-up. To measure the crack opening width, for each specimen, one LVDT was installed at the middle of the notched surface, see Figure 9(b).

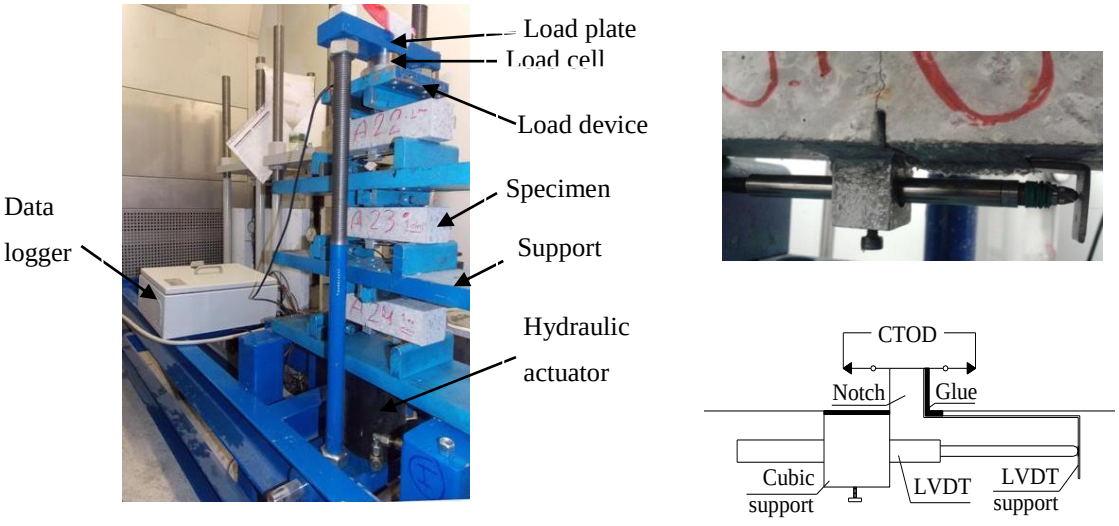

(a) (b)

Figure 9. Creep test setup: (a) general view, (b) position and connection details of the LVDT.

When the variation of the crack opening value was smaller than one micrometer for three consecutive days, it was assumed that the crack opening was stabilized, and then the test was finalized. In the present research, for each creep frame, beams where positioned and loaded according to the following methodology: the beam with the highest value of F_{cr} (the load corresponding to w_{cr}) was placed on the bottom, with a moderate F_{cr} was localized in the middle, and with the lowest F_{cr} was placed on the top. Then, they were loaded, F_a , simultaneously with the smallest F_{cr} value of these three tested specimens.

Post-creep stage

After the end of the creep tests and one week waiting period in order to enable creep deformation recovery, monotonic four-point bending tests were carried out until a 4 mm crack mouth opening width has been reached. The monotonic test set-up was similar to the one used for pre-cracking the beams.

3.3. Results and discussion

3.3.1. Instantaneous four-point bending test

Figure 10 depicts the average and envelope experimental force – crack tip opening displacement relationships. In general, the specimens have shown a linear response up to the load corresponding to the crack initiation. A similar load value at the limit of proportionality was observed for all the series. After the crack initiation, the series with the notched plane more parallel towards to the concrete flow direction, i.e. [0-15°[and [15- 45°[series, showed a higher residual force, and therefore a larger energy absorption capacity than the specimens with a fracture surface more perpendicular to the flow direction.

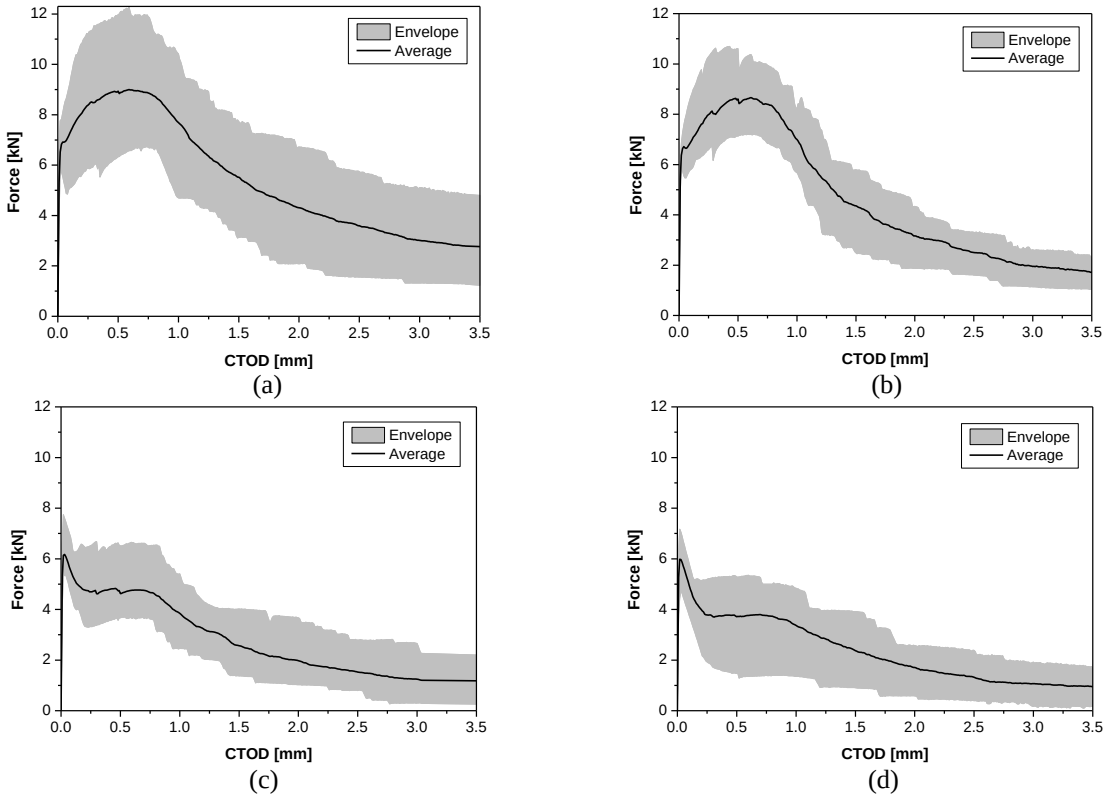

Figure 10. Instantaneous four-point force – crack tip opening displacement response for β in the intervals: (a) [0-15°[, (b) [15-45°[, (c) [45-75°[and (d) [75-90°].

As the angle β increased, fibres tended to be oriented more parallel to the crack plane. This could be justified due to the uniform velocity profile of concrete, which diffuses radially and outwards from the centre of panel. When casting a panel from its centre, fibres tend to have a preferential orientation perpendicular to the concrete flow direction [3, 14]. Therefore, in β=[0-15°] series, the specimens contained more effective fibres that intersected the cracked plane with a lower orientation angle than the other series.

3.3.2. Long-term four point bending test

For the sake of simplicity, the specimens were categorized according to their applied loading level. Two distinct intervals were adopted, namely, [50-75%[and [75-100%] with an average values of 62.5 and 87.5%, and designated as low and high grade F_a/F_{cr} ratios, respectively. Figure 11 depicts the relationship between creep coefficient and time for the studied w_{cr} and F_a/F_{cr} ratios, up to a period of two months. The creep coefficient parameter in the creep stage (φ^C) was calculated by the following equation:

$$\phi^C = w_{lt}/w_{inst} \quad (1)$$

where w_{inst} is the instantaneous crack opening at the time of loading, and w_{lt} represents the long-term crack opening. The creep curves were obtained by averaging the responses in each correspondent category. All series showed a two-stage creep response, namely, the so-called primary and secondary stages. The creep coefficient became stabilized within the studied time period, considering the criterion for stabilized creep, already indicated. During the execution of the test, none of the beams entered into the tertiary creep stage, in which a specimen fails due to creep. In general, the creep coefficient was approximately 48% and 64% higher for the high load level compared to the lower load level, respectively, regarding w_{cr}=0.3 and 0.5 mm series.

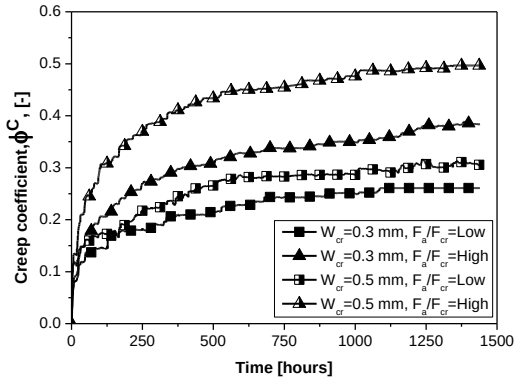

Figure 11. Creep coefficient versus time in the creep tests for the two pre-crack width levels grouped in low and high F_a/F_{cr} ratios.

Regarding the influence of the pre-crack width on the creep coefficient, series with a w_{cr}= 0.5 mm, loaded with a high F_a/F_{cr} ratio had 30% higher creep coefficient than the one of the w_{cr}=0.3 mm series for the same level of loading. By considering the micro-mechanical behaviour of a single fibre, the w_{cr}=0.5 series was submitted to higher damage level of fibre/matrix interface, which led to a higher increase of the crack opening width under a sustained load.

Figure 12 presents the influence of the notched plane orientation (relative to the flow direction of SFRSCC) on the creep coefficient – time relationship. These responses were determined by averaging the curve of the specimens with F_a/F_{cr} = 100%. For the w_{cr} = 0.3 mm series, the variation of creep with time was slightly affected by the direction of the notched plane regarding the expected concrete flow, while in the w_{cr}=0.5 mm series this influence was more significant, confirming the results obtained at micro-mechanical level. In the case of the β=[0-15°[series, the creep coefficient at the end of two months was 13 and 31% higher than in β=[75-90°] for the w_{cr}=0.3 and 0.5 mm series, respectively.

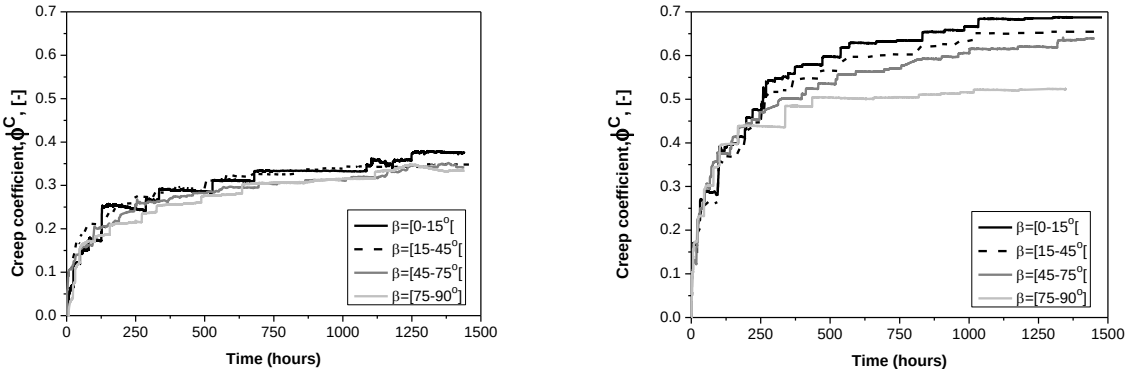

(a) (b)

Figure 12. Creep coefficient versus time for different orientation of the notched plane in the series: (a) w_{cr}=0.3 mm, (b) w_{cr} =0.5 mm.

3.3.3. Comparison between instantaneous and long-term results

Figure 13 compares the long-term assembled curves obtained in four-point bending tests with the correspondent ones determined in the instantaneous tests. In this work, only the results for the high loading level specimens are presented, since they were the most critical ones. These curves were obtained by averaging all responses. The long-term assembled curves consist of overlaying the force – CTOD curves from the tests corresponding to: specimen's pre-cracking, creep, and post-creep. From the analysis of these results, in general, it was concluded that the crack growth during the creep tests has a minor influence on the post-creep flexural behaviour, confirming the results obtained in the fibre pull-out tests. In fact, it is evident that the assembled curves resemble quite well the average response from the instantaneous tests. Nevertheless, in some cases, due to the results' scatter, as consequence of distinct fibre distributions, the assembled responses did not follow so closely the average instantaneous curves, but nonetheless, they were yet contained within the experimental envelope of the instantaneous flexural tests.

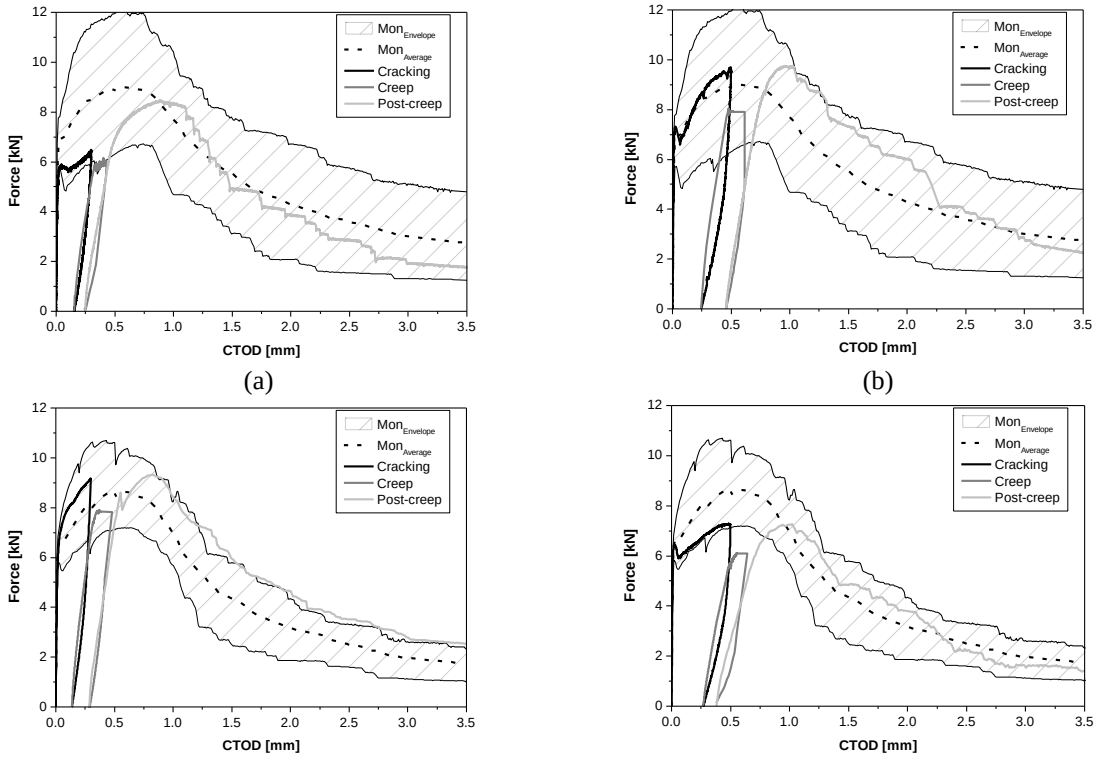

(a) (b)

(c) (d)

Figure 13. Comparison of the instantanous and long-term assembled curves for high level of loading, $75\% < F_a / F_{cr} \leq 100\%$: (a), (b) β = [0-15°]; (c), (d) β = [15-45°]; (e), (f) β = [45-75°]; (g), (h) β = [75-90°]. (a), (c), (e), (g) w_{cr}=0.3 mm and (b), (d), (f), (h) w_{cr}=0.5 mm.

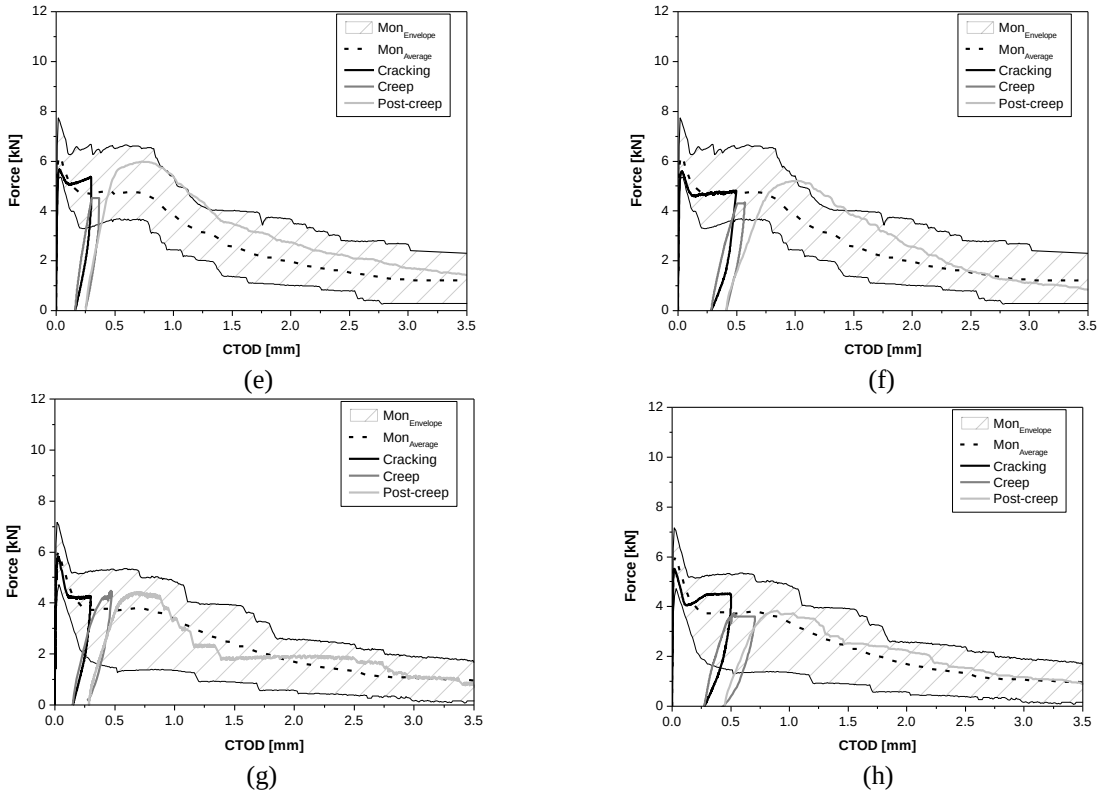

Figure 13 (continue). Comparison of the instantanous and long-term assembled curves for high level of loading, $75\% < F_a / F_{cr} \leq 100\%$: (a), (b) β = [0-15°]; (c), (d) β = [15-45°]; (e), (f) β = [45-75°]; (g), (h) β = [75-90°]. (a), (c), (e), (g) w_{cr}=0.3 mm and (b), (d), (f), (h) w_{cr}=0.5 mm.

4. CONCLUSIONS

Considering the long-term micro-mechanical behaviour for both investigated pre-slip levels, i.e. 0.3 and 0.5 mm, stable responses were obtained for all series. Regarding the influence of the pre-slip levels, s_{pr}= 0.5 mm series showed a higher long-term slip comparing to the s_{pr}= 0.3 mm series. For the s_{pr}= 0.5 mm series, the interface bond between fibre and matrix was more deteriorated, therefore the long-term slip has increased at a higher rate. Moreover, the creep behaviour of the specimens was influenced by the fibre orientation angle. For the time period considered (60 days), fibres with 0° orientation angle showed the highest long-term slip, whereas the lowest long-term slip was observed for the 60° specimens. This was due to the different failure modes of these specimens.

Regarding the long-term composite behaviour, two pre-cracking levels (w_{cr}) were considered. Stable responses were observed for all specimens. Regarding the influence of the pre-cracking levels, w_{cr}=0.5 mm series led to higher values of the creep coefficient than for the w_{cr}=0.3 mm series, especially, if they were loaded with a high F_a / F_{cr}. On the other hand, since w_{cr}=0.5 mm was very close to the CTOD correspondent to the maximum load at the post-cracking branch of the monotonic responses, the bond interface between fibre and matrix was more damaged, therefore the creep crack width increased with a higher rate. Furthermore, the creep tests also revealed that the long-term behaviour of SFRSCC was influenced by the orientation of the notch plane regarding the expected concrete flow (defined by the β angle). In fact, β=[0-15°[specimens presented the highest creep coefficients, whereas β=[75-90°] series showed the lowest ones. This fact was a direct consequence of the fibre orientation within the panel.

ACKNOWLEDGMENTS

This work is supported by the FEDER funds through the Operational Program for Competitiveness Factors - COMPETE and National Funds through FCT - Portuguese Foundation for Science and

Technology under the project SlabSys-HFRC-PTDC/ECM/120394/2010. The materials were supplied by Radmix and Maccaferri (fibres), SECIL (cement), SIKA and BASF (superplasticizers), Omya Comital (limestone filler), and Pegop (Fly ash). The authors also would like to acknowledge the Civitest Company for the development of the Steel Fibre Reinforced Self-Compacting Concrete used in this work.

REFERENCES

[1] Barnett, S.J., Lataste, J.F., Parry, T., Millard, S.G., Soutsos, M.N. (2010). Assessment of fibre orientation in ultra-high performance fibre reinforced concrete and its effect on flexural strength. *Materials and Structures*,43, 1009-1023.
[2] Kang, S.T., Kim, J.K. The relation between fibre orientation and tensile behavior in an ultra high performance fiber reinforced cementitious composite (UHPFRCC). *Cement and Concrete Research*, 41 1001-1014.
[3] Abrishambaf, A., Barros, J.A.O., Cunha, V.M.C.F. (2013). Relation between fibre distribution and post-cracking behaviour in steel fibre reinforced self-compacting concrete panels. *Cement and Concrete Research*,51, 57-66.
[4] Abrishambaf, A., Barros, J.A.O., Cunha, V.M.C.F. (2015). Tensile stress-crack width law for steel fibre reinforced self-compacting concrete obtained from indirect (splitting) tensile tests. *Cement and Concrete Composites*,57, 153-165.
[5] Boshoff, W.B., Mechtcherine, V., van Zijl, G.P.A.G. (2009). Characterizing the time-dependant behaviour on the single fibre level of SHCC: Part 1: Mechanism of fibre pull-out creep. *Cement and Concrete Research*,39, 779-786.
[6] Arango, S.E., Serna, P., Marti-Vargs, J.R. (2012). A test method to characterize flexural creep behaviour of pre-cracked FRC specimens. *Experimental Mechanics Journal*,52, 1067-1078.
[7] Abrishambaf A. Creep behaviour of cracked steel fibre reinforced self-compacting concrete laminar structures. PhD Thesis, University of Minho, Guimarães, Portugal, 2014.
[8] EFNARC. The European guidelines for self-compacting concrete, 2005.
[9] Cunha, V.M.C.F., Barros, J.A.O., Sena-Cruz, J.M. (2011). An integral approch for modelling the tensile behaviour of steel fibre reinforced self-compacting concrete. *Cement and Concrete Research*,41, 64-76.
[10] Stroeven, P., Hu, J. (2006). Effectivness near boundaries of fibre reinforcement in concrete, *Materials and Structures*,39, 1001-1013.
[11] Costa, I.G., Barros, J.A.O. (2015). Tensile creep of a structural epoxy adhessive: experimental and analytical characterization. International Journal of Adhesion and Adhesive,59, 115-124.
[12] UNI11039. Steel fibre reinforced concrete, Part I: Definition, classification, specification and conformity, Part II: Test method for measuring first crack strength and ductility indexes, Italian Board for Standardization, 2003.
[13] CEB-FIP. Volume 1, Model Code 2010, Tomas Telford, Lausanne, Switzerland, 2012.
[14] Abrishambaf, A., Barros, J.A.O., Cunha, V.M.C.F. (2012). Assessment of fibre orientation and distribution in steel fibre reinforced self-compacting concrete panels. 8th RILEM International Symposium on Fibre Reinforced Concrete: Challenges and Opportunities (BEFIB), Guimaraes, Portugal.